Revised chronology of central Tibet uplift (Lunpola Basin)

Xiaomin Fang, Guillaume Dupont-Nivet, Chengshan Wang, Chunhui Song, Qingquan Meng, Weilin Zhang, Junsheng Nie, Tao Zhang, Ziqiang Mao, Yu Chen

▶ **To cite this version:**

Xiaomin Fang, Guillaume Dupont-Nivet, Chengshan Wang, Chunhui Song, Qingquan Meng, et al.. Revised chronology of central Tibet uplift (Lunpola Basin). Science Advances , 2020, 6 (50), pp.eaba7298. 10.1126/sciadv.aba7298 . insu-03051597

HAL Id: insu-03051597
https://insu.hal.science/insu-03051597

Submitted on 10 Dec 2020

HAL is a multi-disciplinary open access archive for the deposit and dissemination of scientific research documents, whether they are published or not. The documents may come from teaching and research institutions in France or abroad, or from public or private research centers.

L'archive ouverte pluridisciplinaire **HAL**, est destinée au dépôt et à la diffusion de documents scientifiques de niveau recherche, publiés ou non, émanant des établissements d'enseignement et de recherche français ou étrangers, des laboratoires publics ou privés.

Distributed under a Creative Commons Attribution 4.0 International License

GEOLOGY

Revised chronology of central Tibet uplift (Lunpola Basin)

Xiaomin Fang[1,2,3]*, Guillaume Dupont-Nivet[4,5], Chengshan Wang[6], Chunhui Song[7], Qingquan Meng[7], Weilin Zhang[1,2], Junsheng Nie[3], Tao Zhang[2], Ziqiang Mao[2], Yu Chen[7]

Copyright © 2020 The Authors, some rights reserved; exclusive licensee American Association for the Advancement of Science. No claim to original U.S. Government Works. Distributed under a Creative Commons Attribution NonCommercial License 4.0 (CC BY-NC).

Knowledge of the topographic evolution of the Tibetan Plateau is essential for understanding its construction and its influences on climate, environment, and biodiversity. Previous elevations estimated from stable isotope records from the Lunpola Basin in central Tibet, which indicate a high plateau since at least 35 Ma, are challenged by recent discoveries of low-elevation tropical fossils apparently deposited at 25.5 Ma. Here, we use magnetostratigraphic and radiochronologic dating to revise the chronology of elevation estimates from the Lunpola Basin. The updated ages reconcile previous results and indicate that the elevations of central Tibet were generally low (<2.3 km) at 39.5 Ma and high (3.5 to 4.5 km) at ~26 Ma. This supports the existence in the Eocene of low-elevation longitudinally oriented narrow regions until their uplift in the early Miocene, with potential implications for the growth mechanisms of the Tibetan Plateau, Asian atmospheric circulation, surface processes, and biotic evolution.

INTRODUCTION

Knowledge of the evolution of the elevation of the Tibetan Plateau is crucial for understanding its growth mechanisms (*1*–*4*), as well as of climatic, environmental, and biotic evolution during the Cenozoic (*5*–*9*). End-member tectonic models predict different uplift histories for different parts of the plateau [e.g., (*1*–*4*)]. Tibetan Plateau uplift is regarded as a primary driver of Cenozoic climatic cooling and Asian monsoon evolution (*1*, *5*, *6*, *10*, *11*), and the Tibetan Plateau is also well suited for studying the evolution of mountain ecosystems [e.g., (*9*, *12*–*14*)]. Thus, a comprehensive understanding of its elevation history can potentially elucidate several important geological and biological issues.

The Lunpola Basin is a prime location for determining the elevation history of the Tibetan Plateau. It is located in the central part of the plateau, and its sedimentary deposits are estimated to range in age from Eocene to Late Miocene (*15*–*18*), spanning most of the interval covering the collision of India and Asia and the resulting tectonic deformation and plateau growth. Continuous fluviolacustrine sedimentary outcrops contain rich and well-preserved fossil assemblages as well as pristine pedogenic carbonate and organic-rich horizons that have been used to infer paleoelevations (*9*, *19*–*24*).

However, previous studies have reached contradictory conclusions regarding the paleoelevation history of central Tibet (*25*). A recent study of fossil palm leaves recovered from the strata of the Lunpola Basin suggested that the elevation of central Tibet was low (<2300 m above mean sea level) until the inferred 25.5-Ma age of these strata (*19*). This challenges previous interpretations of high elevations recovered from the Lunpola Basin strata estimated to be of Eocene age (*3*, *20*, *21*). These findings, which have major implications for understanding the growth mechanisms of the plateau, rely on stratigraphic age interpretations that remain unexpectedly poorly constrained despite the importance of the records (*15*–*18*).

Here, we report new stratigraphic age constraints from a thick sedimentary sequence in the Lunpola Basin including the location of the discovered fossil palm leaves. The results enable a substantial revision of the ages of elevation estimates throughout the Lunpola Basin stratigraphy. The recalibrated elevation history is compared to a regional compilation of elevation records and used to reconsider the growth history of the Tibetan Plateau.

Geological setting

The Lunpola Basin straddles the Bangong-Nujiang suture (BNS) that separates the Lhasa terrane from the Qiantang terrane (*26*) and is bounded by the Tanggula ranges to the north and the Gangdese Arc ranges to the south. It was formed by the rejuvenation of the BNS in response to far-field compression, possibly related to the India-Asia collision and changes in the Neo-Tethyan slab subduction beneath Asia (*26*–*28*). The basin contains 4000- to 5000-m-thick sequences of lacustrine to alluvial sediments generally interpreted to have been deposited in a compressional tectonic setting initiated in the Late Cretaceous–Early Eocene and reactivated by thrusting in the Early Miocene (*26*, *27*). Recent PetroChina seismic surveys and drilling exploration for oil and gas in the basin [e.g., (*28*, *29*)] suggest some degree of local initial extension within the basin, followed by a change to compression in the Neogene (Fig. 1A) (*30*) leading to the thrusting and folding of these sediments along the northern and southern basin margins, which have exposed continuous stratigraphic sequences (Fig. 1B).

The Lunpola Cenozoic sedimentary sequences consist of the Niubao (NB) Formation (estimated Paleocene to Oligocene in age) that grades into the overlying Dingqinghu (DQH) Formation (estimated Oligocene to Early Miocene in age) (*15*, *16*, *28*–*32*). The NB Formation, ~2000 to 3000 m thick, is generally deep red in color and consists of three members: The lower member consists of brownish red conglomerates, sandstones, and siltstone, interpreted as an alluvial fan or a fan delta environment and is only exposed in the western basin along the Zagya Zangbo (river) (fig. S1) and in petroleum boreholes. The middle member consists of reddish to brownish mudstones, intercalated with thin-bedded fine sandstone, shale, and distinct belted white marlite in basin margins, as captured in our measured section; it is interpreted mainly as a shallow lake

[1]Center for Excellence in Tibetan Plateau Earth Sciences, Chinese Academy of Sciences (CAS), Beijing 100101, China. [2]Key Laboratory of Continental Collision and Plateau Uplift, Institute of Tibetan Plateau Research, Chinese Academy of Sciences (CAS), Beijing 100101, China. [3]MOE Key Laboratory of Western China's Environment and College of Resources and Environment, Lanzhou University, Lanzhou 730000, China. [4]Institute of Geosciences, Potsdam University, 14476 Potsdam, Germany. [5]Géosciences Rennes-UMR CNRS 6118, Université de Rennes, 35000 Rennes, France. [6]State Key Laboratory of Biogeology and Environmental Geology, Research Center for Tibetan Plateau Geology, China University of Geosciences (Beijing), Beijing 100083, China. [7]School of Earth Sciences and Key Laboratory of Western China's Mineral Resources of Gansu Province, Lanzhou University, Lanzhou 730000, China. *Corresponding author. Email: fangxm@itpcas.ac.cn

Downloaded from http://advances.sciencemag.org/ on December 10, 2020

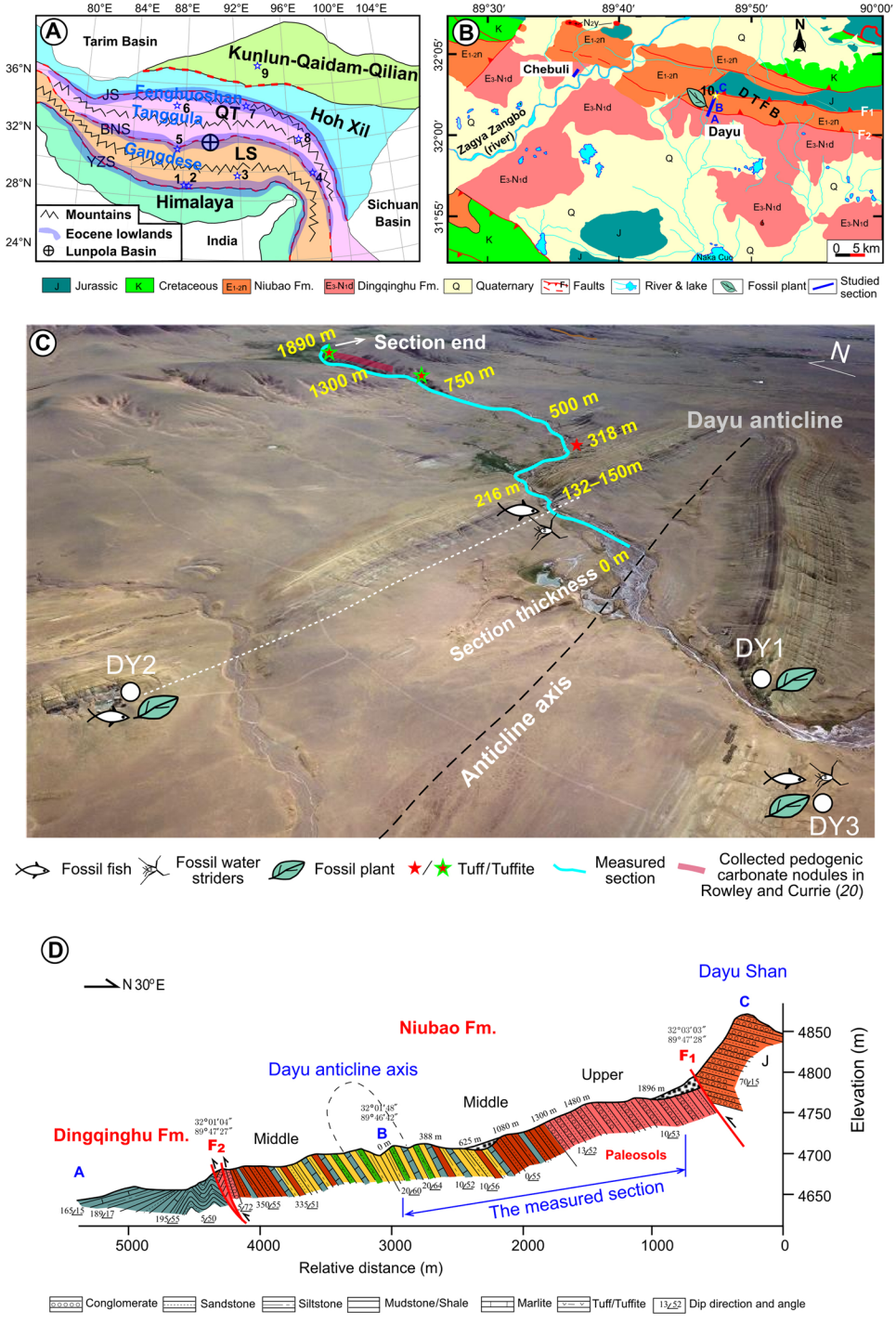

Fig. 1. Tectonic, geological and geomorphological maps showing location of the studied region and sections. (**A**) Location of the Lunpola Basin within the Tibetan Plateau terranes. (**B**) Locations of the studied stratigraphic sections at Dayu and Chebuli on a local geological map of the Lunpola Basin. (**C**) Unmanned aerial vehicle photograph of the Dayu section. (**D**) Cross section showing the relationship between the measured section and the reversed anticline with propagation faults. (A) Paleoelevation features (lowlands and mountains) in the Paleogene are schematically indicated, including numbered points locating the main paleoelevation study sites. 1, Liuqu; 2, Qiabulin; 3, Linzhou; 4, Markam; 5, Nima; 6, Heihuling; 7, Fenghuoshan-Tuotuohe; 8, Nangqian; 9, Qaidam; LS, Lhasa terrane; QT, Qiangtang terrane; YZS, Yalu-Zangbo suture; JS, Jinshajiang suture; DTFB, Dayushan thrust-fold belt. Note that sites DY1 and DY2 bearing fossil palms from the work of Su *et al.* (*19*) belong to the same horizon repeated on either limbs of the Dayu anticline and lie at thicknesses of ~130 to 150 m in the measured Dayu section. In these stratigraphic horizons, we report fish and insect fossils similar to those reported from sites DY1 to DY3. Other sites from which fossil fish, insects, megaplants, and pollen data published in (*25*–*27*), designated DY3, lie at a thickness of ~450 m in the measured section for further age assignment. (B) 10 is the sampling site of Rowley and Currie (*20*). (D) Major faults recognized in the field are a south-verging thrust F1 truncating the NB Fm and F2 placing the sequence upon the DQH Fm. Note that there are no faults affecting the stratigraphy in the measured section.

Downloaded from http://advances.sciencemag.org/ on December 10, 2020

environment. In the basin center, the lithology changes to dominantly brownish greenish siltstone, mudstone, and shale, intercalated with thin sandstone beds and tuffs, interpreted as shallow to deep lake environments. The upper member, in the basin margin, including our measured section, consists of brownish grayish conglomerates, sandstones, and brownish red mudstone, intercalated with markedly reddish luvic paleosols. It is interpreted as a braided river or fan delta. In the basin center, the lithology of this upper member is characterized by brownish mudstone to fine sandstone intercalated with marls and is interpreted as a shallow lake with a subaqueous fan delta. The NB Formation grades into the DQH Formation; it is ~800 to 1000 m thick and is characterized by greenish to grayish mudstones and shale, intercalated with some (~10%) reddish brown mudstone in the upper part and in the basin margins. It is interpreted mainly as deeper to shallower lake environments.

The NB Formation is well exposed in the northern part of the Dayushan thrust-fold belt in the northern margin of the Lunpola Basin where the fossil leaves, paleosols, and our sampling section are located (the Dayu section; Fig. 1, B to D). The DQH Formation crops out in the southern part of the Dayushan thrust-fold belt where the previously studied Chebuli section is located in its western part (Fig. 1B and fig. S1). Here, we focus on the stratigraphy of the NB Formation, which despite being poorly dated is the key to understanding the history of Tibetan topography and uplift mechanisms and thus has become a focus of attention (*20*–*24*).

RESULTS

Chronostratigraphy

Sampling for magnetostratigraphy and tephra was performed along a continuous gully outcrop (called the Dayu section) cutting through the northern limb of the Dayu anticline in the Dayushan thrust-fold belt, where the fossil leaves and paleosols were found. The measured strata in this section are 1890 m thick, continuous from the anticlinal core to the northern limb margin, and truncated by a south-verging thrust; they contain the middle and upper members of the NB Formation (Figs. 1C and 2). About 15 km west of the Dayu section, we also investigated the Chebuli section where the previous stratigraphic age control of the Lunpola Basin was determined (Fig. 1C and fig. S1).

Zircon U-Pb ages were obtained from three volcaniclastic layers from the Dayu section. A ~0.5-m-thick volcaniclastic layer was identified at the 318-m stratigraphic level in the lower part of the Dayu section (Fig. 2C). Its gray color and indurated lithology are clearly distinguishable within a dominantly brownish mudstone sequence. It is massive and contains visible muscovite and biotite (Fig. 2C and fig. S2A). The petrography displays a porphyritic structure where phenocrysts of pyroxene and plagioclase occur randomly within the matrix with a distinct hyalopilitic texture. Some of the volcanic glass has been altered to illite (fig. S2, B and C). Both major and rare earth elements indicate trachyandesite compositions, although there is alteration to K-bentonite (fig. S2D and table S1) (*33*). These features suggest volcanic ash derived from a trachyandesitic eruption. All of the zircon grains exhibit euhedral crystal morphologies with concentric rings indicative of a magmatic origin and with similar ages, with one distinct peak, which yielded an average age of 38.2 ± 0.5 Ma (2σ) (fig. S2, E to G, and table S2). The relatively large age spread around the peak age may suggest reworking or older zircons from the volcanic center that would require using only the youngest grains to constrain the maximum depositional age. However, within the zircon age spread, the following magnetostratigraphic analysis (see below) unequivocally indicates a depositional age (38.1 to 38.4 Ma; C17n.3n) close to the average zircon age (38.2 ± 0.5 Ma), such that the oldest and youngest grains are interpreted as potentially spurious (*34*). At the 1045-m stratigraphic level, in the middle part of the section (Fig. 2), a 0.8-m-thick volcaniclastic layer was identified. It consists of massive brownish gray clayey silts including mica and oxidation spots (fig. S3A). The petrography shows mostly angular quartz, mica, and plagioclase in a silty matrix with a massive and occasionally porous structure infilled with secondary sparry calcite. Illite or weathered mica occurs as convolutive or oriented clumps and aggregates, probably altered from previous glass and large mica grains (fig. S3, C to E). The zircon grains have concentric rings indicative of a magmatic origin (fig. S3B) and have a wide range of U-Pb ages, between 31 and 2760 Ma, with a distinct youngest Oligocene peak yielding a concordant age of 32.4 ± 1.1 Ma (2σ) (fig. S3, F to I, and table S3). At the 1652-m stratigraphic level in the upper part of the section (Fig. 2), another identified volcaniclastic layer, ~0.3 m thick, consists of brownish gray, massive siltstone. The petrography indicates mainly angular quartz grains with larger mica and plagioclase phenocrysts randomly present within a fine matrix (mostly finer quartz, feldspar and weathered aggregated mica, glass, and illite; fig. S4, A to C). Zircon U-Pb dating of this tuffite yielded a relatively wide age spectrum (22.5 to 2729 Ma) but with a well-defined youngest age group with a weighted mean of 23.3 ± 0.3 Ma (2σ) from zircon grains with original euhedral and concentric-ringed crystals indicative of a magmatic origin (fig. S4, D to H, and table S4). This age is consistent with the widespread occurrence of the Early Miocene volcaniclastic layers over the basin (*17*, *18*, *35*). It may correlate in age (Fig. 1C) to a tuffite in the Chebuli section with reported concordant zircon U-Pb ages of 22.57 ± 0.48 Ma (*18*) and 23.6 ± 0.2 Ma (*17*) and with our measured tuff zircon U-Pb age of 23 ± 0.4 Ma (2σ) (figs. S1 and S5 and table S5).

Detailed paleomagnetic sampling was performed at 2- to 5-m intervals along the Dayu section (Figs. 1C and 2). Stepwise thermal demagnetization was applied to two sets of specimens (total of 915) from the collected samples. Well-defined characteristic remanence magnetization (ChRM) directions were recognized for most samples (fig. S6), which pass the reversal test (fig. S7). On the basis of virtual geomagnetic polarity (VGP) latitudes (Fig. 2), 26 pairs of normal (N1 to N26) and reverse (R1 to R26) magnetic polarities are observed (Fig. 2).

Constrained by the three independent zircon U-Pb ages in the lower, middle, and upper parts of the section, respectively, the observed magnetic polarities are readily correlated with chrons 6Bn-19r of the geomagnetic polarity time scale (*36*), yielding the age range of 41.8 to 21.5 Ma for the measured section (Fig. 2). The lower lacustrine portion is especially reliably dated with unequivocal one-to-one correlations of polarity zones R25 to R11 to chrons C18n.2n to C8r (40 to 26 Ma ago). The upper fluvial to alluvial interval includes a few ambiguous correlations and implies that some short chrons are missing, possibly associated with a depositional hiatus typical of these environments, including erosion surfaces and paleosol development; however, the general pattern is clear and concurs with the maximum depositional age of the tuffite.

The resulting sediment accumulation rates are generally uniform and relatively low during the lacustrine-dominated interval, until a threefold increase at 25 Ma ago in the youngest part, characterized by coarser braided river deposits (fig. S8). This pattern is consistent with

Downloaded from http://advances.sciencemag.org/ on December 10, 2020

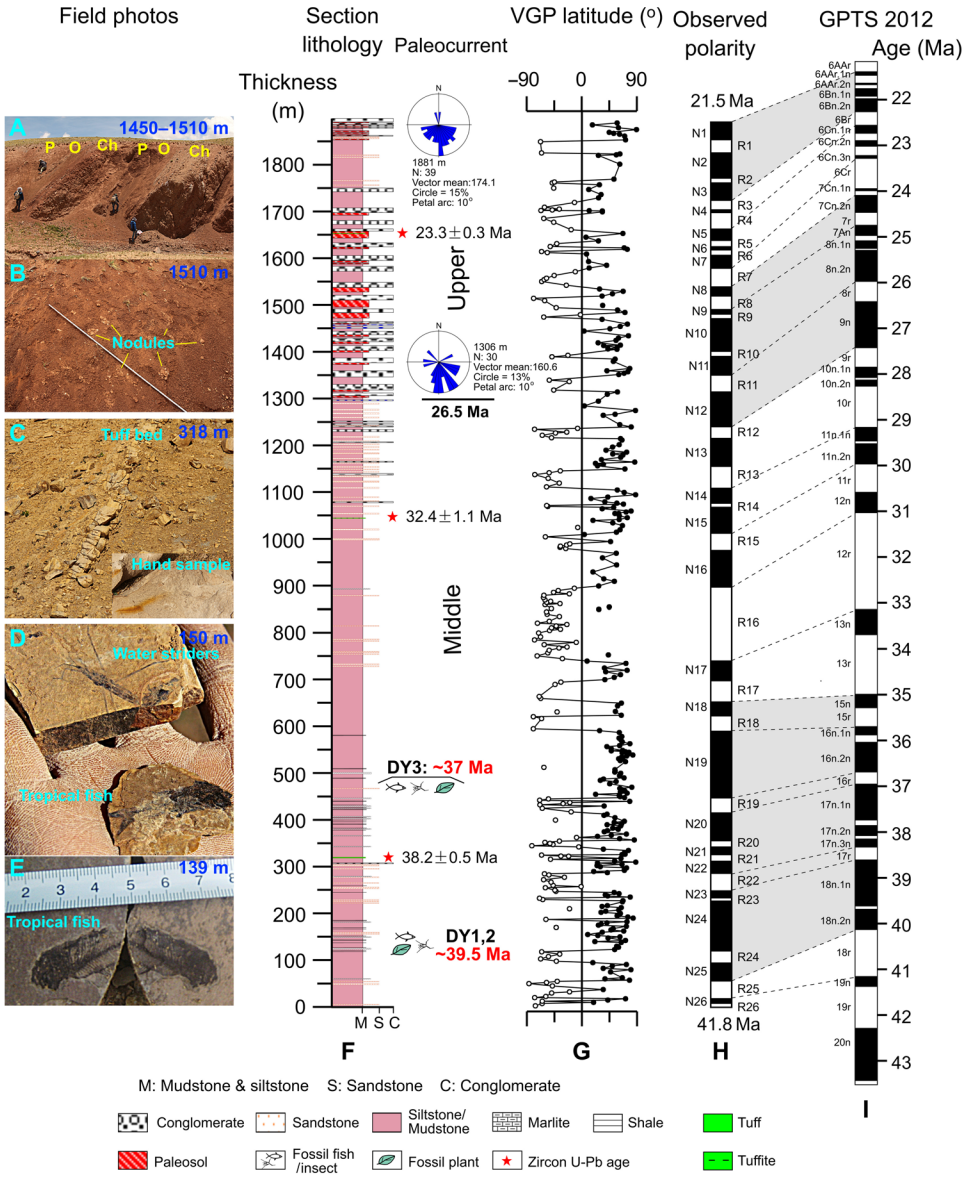

Fig. 2. Correlation of the observed magnetic polarity zones of the measured Dayu section on the northern limb of the Dayu anticline with the geomagnetic polarity time scale (*36*) based on tuff zircon U-Pb age constraints. This yields ages of ~42 to 22 Ma for the measured section, which reassign the age of the fossil palms from the work of Su *et al.* (*19*) to ~39.5 Ma. Other fish, insect, and plant fossils from the works of Wu *et al.* (*22*), Cai *et al.* (*23*), and Jiang *et al.* (*24*) are reassigned an age of ~37 Ma, and the paleosols in the upper section are reassigned an age of ~26.5 to 22 Ma, according to our new age model. Sites DY1, DY2, and DY3 are shown on Fig. 1C. Paleocurrent directions from clast imbrications. (**A**) Paleosol complexes developed on the top of each cycle of channel deposition (conglomerates): overbank deposits (siltstones-mudstones) of a braided river environment. (**B**) Paleosol nodules in luvic paleosol complexes. (**C**) Tuff layer at the thickness of 318 m. (**D**) Tropical water striders and fish (climbing perch) found in shales at the thickness of 150 m. (**E**) Tropical fish (climbing perch) found in grayish shale at the thickness 139 m. (**F**) Schematic lithologic log of the composite section showing stratigraphic positions of paleo-current measurements, radiogenic dating samples and fossils within the Middle and Upper members of the Niubao Formation. (**G**) Virtual Geomagnetic Pole latitudes from paleomagnetic samples throughout the section. Open (full) dots indicate reversed (normal) polarity directions. (**H**) Polarity zones (N for Normal and R for Reversed) inferred from VGP latitudes. Top and basal estimated ages are from correlations to the GPTS indicated by dashed lines to the panel I on the right. (**I**) Geomagnetic Polarity Time Scale (*36*). GPTS, geomagnetic polarity time scale. Photo credit: Xiaomin Fang, ITP, CAS.

the previously inferred tectonic setting of slow subsidence in the Eocene-Oligocene and distal deposition until 26 to 20 Ma ago when basin reactivation and thrusting were associated with proximal facies and regional compressive deformation (*26*, *27*, *37*, *38*). Paleocurrents (fig. S8) from the north suggest uplift north of the Lunpola Basin, probably related to the coeval south-verging Gaize-Amdo thrust belt activity (*18*).

Revision of the Lunpola Basin chronology

In contrast to our direct dating of the strata containing paleoelevation records (stable isotopes and fossil leaves), previous studies [e.g., (*19*, *20*)] had to infer depositional ages on the basis of microfossils (ostracods and palynological assemblages) and an along-strike correlation to the dated Chebuli section (~15 km west of the site; Fig. 1B). For the Chebuli section, 25.5- to 19.8-Ma age

Downloaded from http://advances.sciencemag.org/ on December 10, 2020

constraints are provided by a dated tuff and magnetostratigraphy from a smaller portion of the section (fig. S1, A to C) (*17*). However, stratigraphic correlation from the Dayu to the Chebuli sections is unreliable because the fossil-bearing strata disappear ~1.4 km west of the fossil site at the Dayu section and cannot be traced to the Chebuli section (Fig. 1 and fig. S9). In addition, at the Chebuli site, the dating was performed on a 350-m interval of the lower DQH Formation, but it cannot be extended to the underlying NB Formation (fig. S1) (*17*). Below this dated section, the stratigraphy is buried by Quaternary river sediments such that the contact with the underlying NB Formation cannot be found. Above the dated section, the DQH Formation is thrusted by the lower part of the NB Formation; the middle and upper parts of the NB Formation, however, are not present, as they have been truncated by another thrust (figs. S1 and S9). On the basis of these observations, it is clear that the stratigraphic position of the NB Formation with respect to the dated portion in the lower DQH Formation cannot be estimated precisely at the Chebuli site. However, Su *et al.* (*19*) estimated that the NB Formation should be stratigraphically correlated ~150 m below the dated portion and therefore proposed an age of ~25.5 Ma. Our results from the Dayu section indicate that the fossil site is ~1000 m stratigraphically below the dated portion and is therefore much older. Furthermore, the age of the high-elevation paleosols collected near the Dayu section (*20*) was based on the roughly estimated Eocene age of the NB Formation, but we now recognize that they are actually from the top of the NB Formation dated to the earliest Miocene.

Our results require a revision of the depositional ages of the fossil palm leaves in the Dayu section, as well as the ages of the subsequent fossils from the Lunpola Basin that have been used to infer the paleoelevations of central Tibet. Various animal and plant fossils have previously been used to infer paleoelevations; they include fish (climbing perch, *Eoanabas thibetana* gen. et sp. nov.), insects (water striders, *Aquarius lunpolaensis*), plant megafossils (golden rain trees, *Koelreuteria lunpolaensis* sp. nov. and *Koelreuteria miointegrifoliola*), and diverse subtropical fossil flora (see site DY3 in Fig. 1C for locations) (*22*–*24*). All of these fossils indicate that tropical-subtropical warm and humid conditions have been used to suggest low elevations (<2.3 km) in central Tibet at ~25 Ma ago using previous age estimates (*22*–*24*). According to our new age model, these fossils are now dated to ~37 to 39.5 Ma ago. In addition, paleoelevation estimates based on paleosol carbonate $\delta^{18}O$ from the Lunpola Basin (*20*) also need to be revised. These results obtained near the Dayu section indicated elevations of ~4.5 km at >35 Ma ago, based on previous age estimates mainly from regional correlations. According to our new results, the depositional ages of the reported paleosol carbonate $\delta^{18}O$ data in the upper NB Formation are constrained to the interval of ~26.5 to 21.5 Ma (Fig. 2), suggesting high elevations in central Tibet at this time (Fig. 3). In summary, our new age constraints on this critical sedimentary sequence in the Lunpola Basin enable us to propose a new elevation chronology for central Tibet: low central Tibetan elevations (<2.3 km) during the Eocene (at least since 39.5 Ma ago) but high elevations (~3.5 to 4.5 km) during the latest Oligocene to Early Miocene (at least since ~26 Ma ago). Our substantially revised age constraints, obtained directly from the site containing the elevation proxies, necessitate the revision of several key records that reconciles regional uplift patterns, hence significantly affecting interpretations of regional plateau growth history and its driving mechanisms.

DISCUSSION

Regional pattern of Tibetan elevations since the India-Asia collision

Our results from the Lunpola Basin enable the reconciliation of the previously discrepant paleoelevation datasets from the Tibetan Plateau region. In particular, the inferred high Eocene elevation in the Lunpola Basin has been the most controversial and difficult to explain. Several explanatory hypotheses have been proposed, including the resetting of stable isotopic systems or the use of an alternative lapse rate provided by climate models (*25*, *39*). However, our results show that the discrepancy has arisen simply from poor age control, assigning older ages to high elevations compared to low elevations. To place our results within a regional chronological framework, we now compare them to the growing number of paleoelevation datasets based on various paleoelevation tools: mostly pedogenic carbonate stable isotopes (e.g., $\delta^{18}O$ and $\Delta47$), biomarkers [e.g., plant wax *n*-alkane stable isotopes δD and glycerol dialkyl glycerol tetraethers (GDGTs)], and fossils (e.g., floral and faunal assemblages, palynology, and leaf morphology). We rely on recent exhaustive data compilations that critically address these proxy limitations: Quade *et al.* (*40*) for stable isotopes exploring tectonodiagenetic resetting, Spicer *et al.* (*25*) for providing a full and critical assessment of fossil proxies, Kapp and Decelles (*41*) for integrating tectonic and geologic constraints, and Botsyun *et al.* (*39*) for integrating paleoclimate configurations affecting the proxies.

These studies indicate distinctive regions of low and high elevations during different periods (Figs. 1A and 3). In the Paleocene-Eocene, they now show a consistent pattern of low elevations in east-west (E-W)–elongated regions within a generally high proto-plateau inherited from previous deformation. At ~25 to 20 Ma ago, these low-elevation regions were uplifted to form an exclusively high plateau more similar to that of today. These studies distinguish three of these E-W lowlands: (i) the South Tibetan lowland, running along the Yalu-Zangbo suture (YZS) with the Gangdese Arc mountains to the north and the Himalaya to the south, which emerged only in the Miocene; (ii) the central Tibetan lowland, including the Lunpola Basin, along the BNS, running between the highlands of the Gangdese Arc and the Lhasa plano to the south and the Tanggula and Fenghuo Shan mountains to the north [note that although the high elevations of the Lhasa plano have been contested (*25*, *42*), we follow the arguments of Kapp and Decelles (*41*) for their existence]; and (iii) the north Tibetan lowlands running along the Tanggula thrust fault and the Jinsha suture, with the Tanggula and Fenghuo Shan mountains to the south and bound to the north by the Kunlun mountains. This north Tibetan lowland region was recently suggested to have been moderately low (~2 km) in the Eocene (*43*–*45*) but was later uplifted to 4 km by at least 24 Ma ago (*21*, *45*). The broad region further north of the Hoh Xil Basin, the Kunlun-Qaidam-Qilian, was probably also relatively low (<1.5 to 2 km) in the Eocene-Oligocene (*46*, *47*), although an Oligocene tectonic exhumation and uplift of the Kunlun mountains (*48*) and a reconstructed Oligocene higher elevation of the Qaidam Basin were reported (*49*). In detail, the data are still sparse and often remain controversial, possibly because of local variability. Increased tectonic and sedimentary evidence and paleoaltimetry suggest that the northeastern Tibetan Plateau was already high in some parts in the Eocene but that it was strongly deformed and rapidly uplifted later, mainly since the Late Miocene (*50*–*53*). We note that the central intermontane lowlands are relatively narrow [<~50 to 100 km, accounting for post-Paleogene thrusting and folding; (*41*) and references therein] compared to the surrounding ranges. We therefore suggest that in the Eocene, central-southern Tibet

Downloaded from http://advances.sciencemag.org/ on December 10, 2020

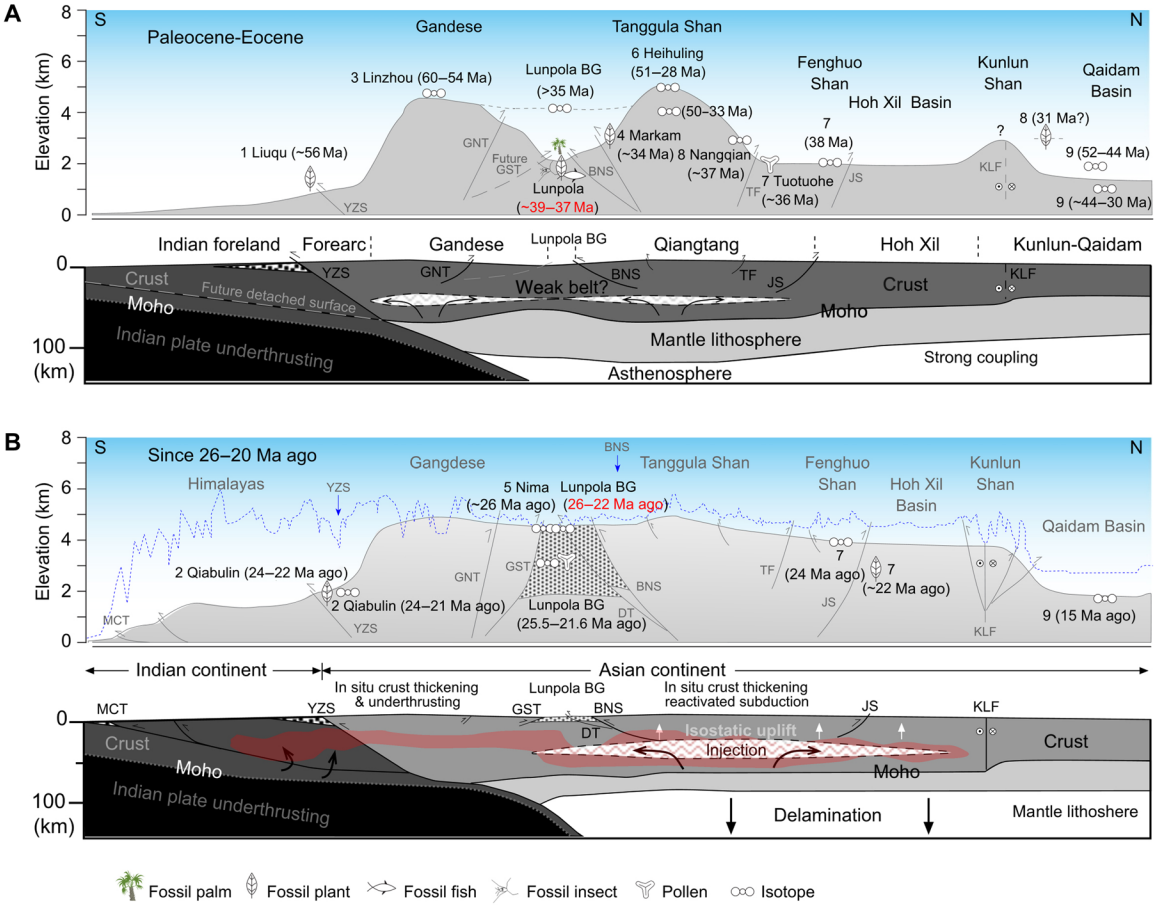

Fig. 3. Schematic diagrams showing the evolution of south-north transects of the topography and the lithospheric and tectonic configurations of southern to central Tibet. (**A**) In the Paleocene-Eocene. (**B**) From the Late Oligocene. The central to southern parts of the plateau are modified from the schematic diagram of Su *et al.* (*19*) and according to revised ages from the Lunpola Basin indicated in red. The age of high elevations estimated from the $\delta^{18}O$ of pedogenic carbonate is revised to the Miocene. The age of fish, insect, and plant fossils indicating low-elevation tropical to subtropical warm and humid environments is now corrected to the Late Eocene, while high stable isotope elevations previously estimated at >35 Ma ago (*20*) are revised here to 26 to 22 Ma ago. The elevation histories of the Liuqu, Linzhou, Qiabulin, Nima, Heihuling, Markam, Hoh Xil, and Qaidam basins (see Fig. 1A for locations) are revised from (*19*, *25*), and those of the Nangqian and Fenghuo Shan basins are revised from (*45*, *76*). The lithospheric and tectonic configurations are estimated on the basis of seismic and tectonic observations of lithospheric structure (*26*–*28*, *30*, *77*–*81*). Lower diagrams show lithospheric scale sketches modified from (*81*–*86*). MCT, Main central thrust; GNT, Gangdese northern margin back thrust; GST, Garze-Seling Co back thrust; DT, Dayushan thrust; KLF, Kunlun fault; BNS (also Shiquanhe-Garze-Amdo thrust system).

was mostly at high elevations, possibly resembling topographically the modern Qaidam to Altai regions with intermontane basins such as the Turpan depression, albeit in a subtropical setting.

Implications for Tibetan plateau growth mechanisms

The Lunpola Basin was initiated as a series of latest Cretaceous to Eocene narrow and partitioned basins along the BNS when the Tanggula thrust belt and the Gangdese retroarc thrust belt were reactivated, with large parts of the northern Lhasa and Qiangtang terranes experiencing rapid exhumation [(*27*, *41*) and references therein]. This far-field compressional deformation phase was also expressed south of the Gangdese mountains, initiating basins along the YZS and extending to the north of the Tanggula mountains, which initiated the Hoh Xil Basin and beyond between the Kunlun ranges bounding the Qaidam Basin [(*41*) and references therein]. Our results confirm that the Lunpola Basin was still at a low elevation in the Eocene and probably stayed low until ~25 Ma ago when the relatively slow subsidence (100 m/Ma) with continuous lacustrine environments were replaced by high sediment accumulation rates and proximal alluvial environments. This suggests that the deformation was limited from ca. 40 to 25 Ma ago; otherwise, such a narrow intermontane basin would have been rapidly consumed. This 15-Ma-long slow lacustrine accumulation is more consistent with postorogenic thermal subsidence (*54*). The location of these basins along the BNS zone led to suggestions of transcontinental subduction or at least reactivation along these preexisting structures during the latest Cretaceous to Eocene (*27*, *55*, *56*). Thermal relaxation of the associated lithospheric mantle thickening may thus explain the Late Eocene–Early Miocene slow subsidence in the Lunpola Basin and possibly at other low elevations and slowly subsiding basins along the suture zones (*57*). Note that some of the basins (e.g., the Kailas Basin) have experienced very rapid infilling followed by uplift, which are recognized as related to different tectonic settings (*38*, *58*, *59*). With respect to the India-Asia collision, this Late Eocene–Early Miocene interval with little deformation and relatively slow subsidence in central Tibet may suggest

Downloaded from http://advances.sciencemag.org/ on December 10, 2020

crustal decoupling from the subducting plate beneath the southern margin of Asia.

The onset at 25 Ma ago of the accumulation of proximal deposits from the north and the documented deformation in the Lunpola Basin is related to the Shiquanhe-Gaize-Amdo thrust-fold system and the Gaize-Seling Co back thrust system. These two systems developed from the BNS and Gangdese back thrust, propagated into the Lunpola and adjacent basins and thrusted and folded them, effectively ending sediment deposition later in the Miocene (Figs. 2 and 3 and fig. S8) (*18*, *27*). This time period corresponds to the regional Early Miocene reactivation of BNS compressive structures throughout the plateau and beyond, with the Himalayan exhumation to the south and extending to relatively distant regions to the north [e.g., the Pamir, Tian Shan, and Qilian Shan; (*41*) and references therein]. This is usually related to subduction of thick Indian continental lithosphere after the Greater India slab break off since the Early Miocene (*60*), as suggested, for example, by plate kinematics that imply that the northern edge of the Indian lithosphere was located near the trench at this time [e.g., (*61*, *62*)]. We can therefore simply attribute the uplift of the low-elevation Tibetan basins to their compressive deformation related to Indian continental subduction. We note, however, that for the Hoh Xil Basin unconformably overlain by flat-lying Miocene lacustrine deposits, there was no important Miocene deformation, suggesting that the uplift more likely relates to lower crustal flow or delamination, as previously indicated [e.g., (*63*)]. Last, the elevation pattern clearly supports two deformation stages that can be compared with models of the India-Asia collision. The quiet Eocene period favors models involving either oceanic subduction of a trans-Tethyan back arc (*41*, *64*) or of a Greater Indian Basin (*65*), with a preference for the latter involving hard Indian collision since 25 to 20 Ma ago. However, we argue that the uplift pattern does not appear to support lower crustal flow as the main driving mechanism of topographic growth before 20 Ma ago for the central lowlands including the Lunpola Basin (Fig. 3 and fig. S8); otherwise, the valleys would have been raised by flow from the surrounding high regions without structures (*66*). That structural deformation appears to have been minimal until the 25– to 20–Ma ago uplift is more likely related to compression, thrusting, and folding rather than to passive uplift (Fig. 3) (*27*, *38*, *41*, *58*, *59*).

Impact on climate, surface processes, and life

Asian atmospheric patterns are well known to be affected by the surface uplift of the Tibetan-Himalayan orogen, which can intensify monsoonal circulation and deflect the westerly jet (*67*). However, we argue that the existence of the narrow E-W lowlands in the Eocene did not substantially affect monsoonal patterns that were likely primarily driven by frontal mountain ranges rather than plateau heating (*7*); these ranges already existed in the Eocene to generate monsoon-like patterns [e.g., (*68*)]. However, climate modeling experiments have yet to test the influence of rugged Eocene paleogeography (*69*). Recent atmospheric modeling experiments (*25*) do not show resulting atmospheric circulations but focus on precipitation stable isotopes in a wide E-W lowland that appears to yield depleted values despite being at low elevations; these depleted values are interpreted to result from a rain shadow effect from the high ranges to the north and south. This provided a valid explanation for the apparently biased Eocene stable isotope values from the Lunpola Basin, but we now show that these values are consistent with high Miocene elevations. Our results indicate that stable isotopic proxies remain generally valid, although climate simulations are needed to better constrain them with realistic atmospheric circulation patterns (*39*). Depleted stable isotope values from these E-W low-elevation regions remain to be documented and would be at odds with fossil evidence and depositional environments indicating moist and warm tropical to subtropical conditions (*25*). We thus argue that substantial moisture was brought to these Eocene E-W lowlands by the westerlies or the East Asian monsoons but these moisture sources were later deflected and/or shielded by frontal ranges upon Early Miocene uplift.

The surface processes associated with these E-W Eocene lowlands remain to be explored. In the Lunpola Basin, the depositional environments are generally lacustrine with low sediment accumulation rates, suggesting underfilled internally drained basins in agreement with paleocurrent orientations (fig. S8) (*18*, *37*, *38*); this suggests no outlet with a sediment contribution to the oceans and, thus, limited drainage incision. However, a strong hydrological cycle may have been promoted by intense evaporation, at least seasonally, which would be expected at these paleolatitudes, and is indicated by the distinctive evaporite/lignite alternations of these basins that are also characteristic of the Eocene deposits in eastern China [e.g., (*59*, *69*, *70*)]. We acknowledge that there is still insufficient evidence to eliminate the possibility that these Eocene drainages were connected to the surrounding seas, either to the east (e.g., the China Seas and proto-Bengal fan) or to the west (e.g., the proto-Paratethys and Neo-Tethys), as suggested by Eocene marine fossils found in the Gerze Basin east of the Lunpola Basin (*71*). Further provenance studies may elucidate these connections to internal Tibetan sources and record their disconnection upon Early Miocene uplift [e.g., (*72*)].

Biotic communities documented by fossils in the Lunpola Basin and other Eocene Tibetan lowlands yield highly diverse tropical-subtropical taxa (*22*–*24*). These relatively isolated lowland habitats surrounded by large elevation gradients were an ideal setting for the development of a biodiverse habitat that may have served as a cradle for specific Tibetan species [e.g., (*9*, *12*, *14*)]. These lowlands have also provided ideal biotic interchange pathways for E-W migrations, potentially promoting exchange between East China/Southeast Asia and Central Asia/Western Asia (*73*, *74*). The 25– to 20–Ma ago uplift of these lowlands must therefore have had a major influence on the origin and evolution of species derived from the Tibetan region that may be traceable in genomic signatures (*9*, *12*–*14*).

The ongoing surge of paleoelevation data from in and around the Tibetan region will enable to better constrain the general patterns and explore other local variations. This is promising for resolving long-standing controversies regarding the formation of the Tibetan Plateau, and they should provide fundamental constraints on its tectonic driving mechanisms and the interactions with surface processes, climate (regional and global), and biotic evolution. Our study demonstrates that reliable age control of these paleoelevation proxies is critical and emphasizes that paleoelevation data integrated with geological, geophysical, and geochemical research, including sedimentological, structural geology, and thermochronological data, are needed to formulate realistic inferences about Tibetan Plateau growth and its driving mechanisms and climatic impacts [(*41*) and references therein].

METHODS

Radiometric dating

Zircons extracted by conventional magnetic and density techniques were mounted in epoxy and polished to expose half of the grains for

Downloaded from http://advances.sciencemag.org/ on December 10, 2020

analysis. Cathodoluminescence images were obtained to check the internal structures and targeting spots for dating. Experiments were performed using an American Agilent 7700x laser ablation inductively coupled plasma mass spectrometer equipped with a 193-nm excimer laser ablation system at the Key Laboratory of Western China's Mineral Resources of Gansu Province, Lanzhou University. The ablated spots are 20 μm in depth and 30 μm in diameter. Isotope ratios were determined related to Harvard zircon 91500, and concentrations were calculated using NIST SRM 610 as an external standard using GLITTER (4.0) software. The corrected $^{206}Pb/^{238}U$ ages were accepted for ages <1000 Ma ago, while $^{207}Pb/^{206}Pb$ ages were accepted for ages >1000 Ma ago. Diagrams of U-Pb concordia and weight average histograms were drawn using Isoplot version 3.0 (*75*).

Paleomagnetic dating

Oriented block samples with dimensions of roughly 10 cm by 10 cm by 8 cm were obtained from the Dayu section. The block samples were then cut into three oriented cubic specimens of dimensions 2 cm by 2 cm by 2 cm in the laboratory. After natural remanent magnetization (NRM) measurements, all specimens were subjected to stepwise thermal demagnetization using an ASD MMTD-48 oven at temperatures ranging from 20° to 700°C or until the intensity of the ChRM was <5% of the NRM. The remanence was measured using a 2G-760R cryogenic magnetometer in a magnetically shielded room at the Paleomagnetism and Rock Magnetism Laboratory in the Ministry of Education Key Laboratory of Western China's Environmental Systems, Lanzhou University, China.

SUPPLEMENTARY MATERIALS

Supplementary material for this article is available at http://advances.sciencemag.org/cgi/content/full/6/50/eaba7298/DC1

REFERENCES AND NOTES

1. P. Molnar, P. England, J. Martinod, Mantle dynamics, uplift of the Tibetan Plateau, and the Indian monsoon. *Rev. Geophys.* **31**, 357–396 (1993).
2. P. Tapponnier, X. Zhiqin, F. Roger, B. Meyer, N. Arnaud, G. Wittlinger, Y. Jingsui, Oblique stepwise rise and growth of the Tibet Plateau. *Science* **294**, 1671–1677 (2001).
3. C. Wang, X. Zhao, Z. Liu, P. C. Lippert, S. A. Graham, R. S. Coe, H. Yi, L. Zhu, S. Liu, Y. Li, Constraints on the early uplift history of the Tibetan Plateau. *Proc. Natl. Acad. Sci. U.S.A.* **105**, 4987–4992 (2008).
4. L. Ding, Q. Xu, Y. Yue, H. Wang, F. Cai, S. Li, The Andean-type Gangdese Mountains: Paleoelevation record from the Paleocene-Eocene Linzhou Basin. *Earth Planet. Sci. Lett.* **392**, 250–264 (2014).
5. W. F. Ruddiman, J. E. Kutzbach, Forcing of late Cenozoic northern hemisphere climate by plateau uplift in southern asia and the American west. *J. Geophys. Res. Atmos.* **94**, 18409–18427 (1989).
6. J. Li, X. Fang, Uplift of the Tibetan Plateau and environmental changes. *Chin. Sci. Bull.* **44**, 2117–2124 (1999).
7. W. R. Boos, Z. Kuang, Dominant control of the South Asian monsoon by orographic insulation versus plateau heating. *Nature* **463**, 218–222 (2010).
8. G. Wu, Y. Liu, B. He, Q. Bao, A. Duan, F.-F. Jin, Thermal controls on the Asian summer monsoon. *Sci. Rep.* **2**, 404 (2012).
9. T. Deng, X. Wang, F. Wu, Y. Wang, Q. Li, S. Wang, S. Hou, Review: Implications of vertebrate fossils for paleo-elevations of the Tibetan Plateau. *Global Planet. Change* **174**, 58–69 (2019).
10. A. Zhisheng, J. E. Kutzbach, W. L. Prell, S. C. Porter, Evolution of Asian monsoons an phased uplift of the Himalaya–Tibetan Plateau since Late Miocene times. *Nature* **411**, 62–66 (2001).
11. Z. T. Guo, W. F. Ruddiman, Q. Z. Hao, H. B. Wu, Y. S. Qiao, R. X. Zhu, S. Z. Peng, J. J. Wei, B. Y. Yuan, T. S. Liu, Onset of Asian desertification by 22 Myr ago inferred from loess deposits in China. *Nature* **416**, 159–163 (2002).
12. A. Favre, M. Päckert, S. U. Pauls, S. C. Jähnig, D. Uhl, I. Michalak, A. N. Muellner-Riehl, The role of the uplift of the Qinghai-Tibetan Plateau for the evolution of Tibetan biotas. *Biol. Rev. Camb. Philos. Soc.* **90**, 236–253 (2015).
13. S. S. Renner, Available data point to a 4-km-high Tibetan Plateau by 40 Ma, but 100 molecular-clock papers have linked supposed recent uplift to young node ages. *J. Biogeogr.* **43**, 1479–1487 (2016).
14. V. Mosbrugger, A. Favre, A. Muellner-Riehl, M. Packert, A. Mulch, Cenozoic evolution of geobiodiversity in the Tibeto-Himalayan Region. *Wiley-Blackwell* **28**, 429–448 (2018).
15. W. Kaifa, Y. Jiaowen, L. Zhe, L. Zengrtji, On the tertiary sporo-pollen assemblages from Lunpola Basin of Xizang, China and their palaeogeographic significance. *Sci. Geol. Sin.* **4**, 366–374 (1975).
16. W.-G. Xia, Ostracode fauna from Lunpola Group in Xizang (Tibet) and its geological age, in *Chinese Geology Bureau Tibetan Plateau Proceeding Editorial Committee (Ed.), Contribution to the Geology of the Qinghai-Xizang (Tibet) Plateau* (Geological Publishing House, 1982), pp. 149–159.
17. J. Sun, Q. Xu, W. Liu, Z. Zhang, L. Xue, P. Zhao, Palynological evidence for the latest Oligocene–early Miocene paleoelevation estimate in the Lunpola Basin central Tibet. *Palaeogeogr. Palaeoclimatol. Palaeoecol.* **399**, 21–30 (2014).
18. Z. Han, H. D. Sinclair, Y. Li, C. Wang, Z. Tao, X. Qian, Z. Ning, J. Zhang, Y. Wen, J. Lin, B. Zhang, M. Xu, J. Dai, A. Zhou, H. Liang, S. Cao, Internal drainage has sustained low-relief Tibetan landscapes since the early Miocene. *Geophys. Res. Lett.* **46**, 8741–8752 (2019).
19. T. Su, A. Farnsworth, R. A. Spicer, J. Huang, F.-X. Wu, J. Liu, S.-F. Li, Y.-W. Xing, Y.-J. Huang, W.-Y.-D. Deng, H. Tang, C.-L. Xu, F. Zhao, G. Srivastava, P. J. Valdes, T. Deng, Z.-K. Zhou, No high Tibetan Plateau until the Neogene. *Sci. Adv.* **5**, eaav2189 (2019).
20. D. B. Rowley, B. S. Currie, Palaeo-altimetry of the late Eocene to Miocene Lunpola basin, central Tibet. *Nature* **439**, 677–681 (2006).
21. P. J. Polissar, K. H. Freeman, D. B. Rowley, F. A. McInerney, B. S. Currie, Paleoaltimetry of the Tibetan Plateau from *D/H* ratios of lipid biomarkers. *Earth Planet. Sci. Lett.* **287**, 64–76 (2009).
22. F. Wu, D. Miao, M.-m. Chang, G. Shi, N. Wang, Fossil climbing perch and associated plant megafossils indicate a warm and wet central Tibet during the late Oligocene. *Sci. Rep.* **7**, 878 (2017).
23. C. Cai, D. Huang, F. Wu, M. Zhao, N. Wang, Tertiary water striders (Hemiptera, Gerromorpha, Gerridae) from the central Tibetan Plateau and their palaeobiogeographic implications. *J. Asian Earth Sci.* **175**, 121–127 (2019).
24. H. Jiang, T. Su, W. O. Wong, F. Wu, J. Huang, G. Shi, Oligocene *Koelreuteria* (Sapindaceae) from the Lunpola Basin in central Tibet and its implication for early diversification of the genus. *J. Asian Earth Sci.* **175**, 99–108 (2019).
25. R. A. Spicer, T. Su, P. J. Valdes, A. Farnsworth, F.-X. Wu, G. Shi, T. E. V. Spicer, Z. Zhou, Why 'the uplift of the Tibetan Plateau' is a myth? *Natl. Sci. Rev.* **2020**, nwaa091 (2020).
26. A. Yin, T. M. Harrison, Geologic evolution of the Himalayan-Tibetan orogen. *Annu. Rev. Earth Planet. Sci.* **28**, 211–280 (2000).
27. P. Kapp, A. Yin, T. M. Harrison, L. Ding, Cretaceous-tertiary shortening, basin development, and volcanism in central Tibet. *Geol. Soc. Am. Bull.* **117**, 865–878 (2005).
28. C.-S. Wang, J.-G. Dai, X.-X. Zhao, Y.-L. Li, S.-A. Graham, D.-F. He, B. Ran, J. Meng, Outward-growth of the Tibetan Plateau during the cenozoic: A review. *Tectonophysics* **621**, 1–43 (2014).
29. Z.-R. Liu, X.-Q. Li, Late tectonic deformation characteristics and stress mechanism in Lunpola Basin, Tibet Plateau. *Pet. Geo. Expl.* **39**, 819–841 (2017).
30. A. Huaguo, L.-Y. Lan, H.-Q. Zhu, K.-Y. Zhang, T. Zeng, The forming mechanism and petroleum geology of Tertiary Lunpola Basin, Tibet. *Acta Pet. Sin.* **19**, 21–27 (1998).
31. Z.-Y. Xu, The Tertiary and its petroleum potential in the Lunpola Basin, Tibet. *Oil Gas Geol.* **1**, 153–158 (1980).
32. L. Qingliang, F. Xiaoyue, L. Yiaping, Petroleum geological features of tertiary terrestrial Lunpola Basin, Xizang (Tibet). *Earth Sci. J. China Univ. Geosci.* **21**, 168–173 (1996).
33. H. Hong, L. Zhao, Q. Fang, T. J. Algeo, C. Wang, J. Yu, N. Gong, K. Yin, Volcanic sources and diagenetic alteration of Permian–Triassic boundary K-bentonites in Guizhou Province, South China. *Palaeogeogr. Palaeoclimatol. Palaeoecol.* **519**, 141–153 (2019).
34. C. Rossignol, E. Hallot, S. Bourquin, M. Poujol, M. Jolivet, P. Pellenard, C. Ducassou, T. Nalpas, G. Heilbronn, J. Yu, M.-P. Dabard, Using volcaniclastic rocks to constrain sedimentation ages: To what extent are volcanism and sedimentation synchronous? *Sediment. Geol.* **381**, 46–64 (2019).
35. Z. Mao, Q. Meng, X. Fang, T. Zhang, F. Wu, Y. Yang, W. Zhang, J. Zan, M. Tan, Recognition of tuffs in the middle-upper Dingqinghu Fm., Lunpola basin, Central Tibetan Plateau: Constraints on stratigraphic age and implications for paleoclimate. *Palaeogeogr. Palaeoclimatol. Palaeoecol.* **525**, 44–56 (2019).
36. F. M. Gradstein, J. G. Ogg, M. D. Schmitz, G. M. Ogg, *The Geologic Time Scale 2012* (Elsevier, ed. 1, 2012).
37. P. G. DeCelles, J. Quade, P. Kapp, M. Fan, D. L. Dettman, L. Ding, High and dry in central Tibet during the late oligocene. *Earth Planet. Sci. Lett.* **253**, 389–401 (2007).
38. P. G. DeCelles, P. Kapp, L. Ding, G. E. Gehrels, Late cretaceous to middle Tertiary basin evolution in the central Tibetan Plateau: Changing environments in response to tectonic partitioning, aridification, and regional elevation gain. *Geol. Soc. Am. Bull.* **119**, 654–680 (2007).

Downloaded from http://advances.sciencemag.org/ on December 10, 2020

39. S. Botsyun, P. Sepulchre, Y. Donnadieu, C. Risi, A. Licht, J. K. C. Rugenstein, Revised paleoaltimetry data show low Tibetan Plateau elevation during the Eocene. *Science* **363**, eaaq1436 (2019).
40. J. Quade, R. Leary, M. P. Dettinger, D. Ormed, A. Krupa, P. G. DeCelles, A. Kano, H. Kato, R. Waldrip, W. Huang, P. Kapp, Resetting Southern Tibet: The serious challenge of obtaining primary records of paleoaltimetry. *Global Planet. Change* **191**, 103194 (2020).
41. P. Kapp, P. G. Decelles, Mesozoic–Cenozoic geological evolution of the Himalayan-Tibetan orogen and working tectonic hypotheses. *Am. J. Sci.* **319**, 159–254 (2019).
42. R. Hetzel, I. Dunkl, V. Haider, M. Strobl, H. von Eynatten, L. Ding, D. Frei, Peneplain formation in southern Tibet predates the India-Asia collision and plateau uplift. *Geology* **39**, 983–986 (2011).
43. A. J. Cyr, B. S. Currie, D. B. Rowley, Geochemical evaluation of Fenghuoshan Group lacustrine carbonates, north-central Tibet: Implications for the paleoaltimetry of the Eocene Tibetan Plateau. *J. Geol.* **113**, 517–533 (2005).
44. Y. Miao, F. Wu, H. Chang, X. Fang, T. Deng, J. Sun, C. Jin, A late-eocene palynological record from the Hoh Xil Basin, northern Tibetan Plateau, and its implications for stratigraphic age, paleoclimate and paleoelevation. *Gondw. Res.* **31**, 241–252 (2016).
45. J. Lin, J.-G. Dai, G. Zhuang, G. Jia, L. Zhang, Z. Ning, Y. Li, C. Wang, Late eocene-oligocene high relief paleotopography in the north central Tibetan Plateau: Insights from detrital zircon U-Pb geochronology and leaf wax hydrogen isotope studies. *Tectonics* **39**, e2019TC005815 (2020).
46. L.-L. Li, C.-D. Wu, C.-F. Fan, J.-J. Li, C.-H. Zhang, Carbon and oxygen isotopic constraints on paleoclimate and paleoelevation of the southwestern Qaidam basin, northern Tibetan Plateau. *Geosci. Front.* **8**, 1175–1186 (2017).
47. B. Song, K. Zhang, L. Zhang, J. Ji, H. Hong, Y. Wei, Y. Xu, T. J. Alego, C. Wang, Qaidam Basin paleosols reflect climate and weathering intensity on the northeastern Tibetan Plateau during the Early Eocene Climatic Optimum. *Palaeogeogr. Palaeoclimatol. Palaeoecol.* **512**, 6–22 (2018).
48. C. Mock, N. O. Arnaud, J.-M. Cantagrel, An early unroofing in northeastern Tibet? Constraints from $^{40}Ar/^{39}Ar$ thermochronology on granitoids from the eastern Kunlun range (Qianghai, NW China). *Earth Planet. Sci. Lett.* **171**, 107–122 (1999).
49. B. Song, R. A. Spicer, K. Zhang, J. Ji, A. Farnsworth, A. C. Hughes, Y. Yang, F. Han, Y. Xu, T. Spicer, T. Shen, D. J. Lunt, G. Shi, Qaidam Basin leaf fossils show northeastern Tibet was high, wet and cool in the early Oligocene. *Earth Planet. Sci. Lett.* **537**, 116175 (2020).
50. X. Fang, D. Liu, C. Song, S. Dai, Q. Meng, *Oligocene Slow and Miocene–Quaternary Rapid Deformation and Uplift of the Yumu Shan and North Qilian Shan: Evidence from High-Resolution Magnetostratigraphy and Tectonosedimentology*, vol. 373 of *Magnetic Methods and the Timing of Geological Processes* (The Geological Society of London, 2013), pp. 149–171.
51. J. Li, X. Fang, C. Song, B. Pan, Y. Ma, M. Yan, Late Miocene–Quaternary rapid stepwise uplift of the NE Tibetan Plateau and its effects on climatic and environmental changes. *Quatern. Res.* **81**, 400–423 (2014).
52. G. Zhuang, M. T. Brandon, M. Pagani, S. Krishnan, Leaf wax stable isotopes from northern Tibetan Plateau: Implications for uplift and climate since 15 Ma. *Earth Planet. Sci. Lett.* **390**, 186–198 (2014).
53. J.-L. Chen, A. Yin, J.-F. Xu, Y.-H. Dong, Z.-Q. Kang, Late Cenozoic magmatic inflation, crustal thickening, and >2 km of surface uplift in central Tibet. *Geology* **46**, 19–22 (2018).
54. D. McKenzie, Some remarks on the development of sedimentary basins. *Earth Planet. Sci. Lett.* **40**, 25–32 (1978).
55. M. S. Spurlin, A. Yin, B. K. Horton, J. Zhou, J. Wang, Structural evolution of the Yushu-Nangqian region and its relationship to syn-collisional igneous activity, east-central Tibet. *Geol. Soc. Am. Bull.* **117**, 1293–1317 (2005).
56. S. Guillot, F. Goussin, L. Airaghi, A. Replumaz, J. de Sigoyer, C. Cordier, How and when did the Tibetan Plateau grow? *Russ. Geol. Geophys.* **60**, 957–977 (2019).
57. B. Sun, Y.-F. Wang, C.-S. Li, J. Yang, J.-F. Li, Y.-L. Li, T. Deng, S.-Q. Wang, M. Zhao, R. A. Spicer, D. K. Ferguson, R. C. Mehrotra, Early Miocene elevation in northern Tibet estimated by palaeobotanical evidence. *Sci. Rep.* **5**, 10379 (2015).
58. P.-G. DeCelles, P. Kapp, J. Quade, G.-E. Gehrels, Oligocene–Miocene Kailas Basin, southwestern Tibet: Record of postcollisional upper-plate extension in the Indus-Yarlung suture zone. *Geol. Soc. Am. Bull.* **123**, 1337–1362 (2011).
59. P. G. DeCelles, B. Carrapa, G. E. Gehrels, T. Chakraborty, P. Ghosh, Along-strike continuity of structure, stratigraphy, and kinematic history in the Himalayan thrust belt: The view from Northeastern India. *Tectonics* **35**, 2995–3027 (2016).
60. P. G. DeCelles, D. M. Robinson, G. Zandt, Implications of shortening in the Himalayan fold-thrust belt for uplift of the Tibetan Plateau. *Tectonics* **21**, 12-1–12-25 (2002).
61. J. Nábělek, G. Hetényi, J. Vergne, S. Sapkota, B. Kafle, M. Jiang, H. Su, J. Chen, B.-S. Huang; Hi-CLIMB Team, Underplating in the Himalaya-Tibet collision zone revealed by the Hi-CLIMB experiment. *Science* **325**, 1371–1374 (2009).
62. P. Molnar, J. M. Stock, Slowing of India's convergence with Eurasia since 20 Ma and its implications for Tibetan mantle dynamics. *Tectonics* **28**, 10.1029/2008TC002271, (2009).
63. L. M. Staisch, N. A. Niemi, M. K. Clark, H. Chang, Eocene to late Oligocene history of crustal shortening within the Hoh Xil Basin and implications for the uplift history of the northern Tibetan Plateau. *Tectonics* **35**, 862–895 (2016).
64. J. C. Aitchison, J. R. Ali, A. M. Davis, When and where did India and Asia collide? *J. Geophys. Res. Solid Earth* **112**, B05423 (2007).
65. D. J. J. van Hinsbergen, P. C. Lippert, G. Dupont-Nivet, N. McQuarrie, P. V. Doubrovine, W. Spakman, T. H. Torsvik, Greater India Basin hypothesis and a two-stage Cenozoic collision between India and Asia. *Proc. Natl. Acad. Sci. U.S.A.* **109**, 7659–7664 (2012).
66. L. Husson, T. Sempere, Thickening the Altiplano crust by gravity-driven crustal channel flow. *Geophys. Res. Lett.* **30**, 1243 (2003).
67. P. Molnar, W.-R. Boos, D.-S. Battisti, Orographic controls on climate and paleoclimate of Asia: Thermal and mechanical roles for the Tibetan Plateau. *Annu. Rev. Earth Planet. Sci.* **38**, 77–102 (2010).
68. L. Ding, R. A. Spicer, J. Yang, Q. Xu, F. Cai, S. Li, Q. Lai, H. Wang, T. E. V. Spicer, Y. Yue, A. Shukla, G. Srivastava, M. A. Khan, S. Bera, R. Mehrotra, Quantifying the rise of the Himalaya orogen and implications for the South Asian monsoon. *Geology* **45**, 215–218 (2017).
69. D. Tardif, F. Fluteau, Y. Donnadieu, G. Le Hir, J.-B. Ladant, P. Sepulchre, A. Licht, F. Poblete, G. Dupont-Nivet, The origin of Asian Monsoons: A modelling perspective. *Clim. Past Discuss.* **16**, 847–865 (2020).
70. D. Wang, S. Lu, S. Han, X. Sun, C. Quan, Eocene prevalence of monsoon-like climate over eastern China reflected by hydrological dynamics. *J. Asian Earth Sci.* **62**, 776–787 (2013).
71. Y. Wei, K. Zhang, C. N. Garzione, Y. Xu, B. Song, J. Ji, Low palaeoelevation of the northern Lhasa terrane during late Eocene: Fossil foraminifera and stable isotope evidence from the Gerze Basin. *Sci. Rep.* **6**, 27508 (2016).
72. P. D. Clift, A. Carter, A. Wysocka, L. V. Hoang, H. Zheng, N. Neubeck, A late eocene-oligocene through-flowing river between the upper Yangtze and South China Sea. *Geochem. Geophys. Geosyst.* **21**, e2020GC009046 (2020).
73. J. Liu, T. Su, R. A. Spicer, H. Tang, W.-Y.-D. Deng, F.-X. Wu, G. Srivastava, T. Spicer, T. Van Do, T. Deng, Z.-K. Zhou, Biotic interchange through lowlands of Tibetan Plateau suture zones during Paleogene. *Palaeogeogr. Palaeoclimatol. Palaeoecol.* **524**, 33–40 (2019).
74. G. J. Vermeij, When biotas meet: Understanding biotic interchange. *Science* **253**, 1099–1104 (1991).
75. K. R. Ludwig, *User's Manual for Isoplot/Ex Version 3.00: A Geochronological Toolkit for Microsoft Excel* (Berkeley Geochronology Center Special Publications, 2003), pp. 1–71.
76. L. Li, M. Fan, N. Davila, G. Jesmok, B. Mitsunaga, A. Tripati, D. Orme, Carbonate stable and clumped isotopic evidence for late Eocene moderate to high elevation of the east-central Tibetan Plateau and its geodynamic implications. *Geol. Soc. Am. Bull.* **131**, 831–844 (2019).
77. R. Gao, C. Chen, Z. Lu, L. D. Brown, X. Xiong, W. Li, G. Deng, New constraints on crustal structure and Moho topography in Central Tibet revealed by SinoProbe deep seismic reflection profiling. *Tectonophysics* **606**, 160–170 (2013).
78. R. Gao, Z. Lu, S. L. Klemperer, H. Wang, S. Dong, W. Li, H. Li, Crustal-scale duplexing beneath the Yarlung Zangbo suture in the western Himalaya. *Nat. Geosci.* **9**, 555–560 (2016).
79. R. Kind, X. Yuan, J. Saul, D. Nelson, S. V. Sobolev, J. Mechie, W. Zhao, G. Kosarev, J. Ni, U. Achauer, M. Jiang, Seismic images of crust and upper mantle beneath Tibet: Evidence for Eurasian plate subduction. *Science* **298**, 1219–1221 (2002).
80. G. Kosarev, R. Kind, S. V. Sobolev, X. Yuan, W. Hanka, S. Oreshin, Seismic evidence for a detached Indian lithospheric mantle beneath Tibet. *Science* **283**, 1306–1309 (1999).
81. T. J. Owens, G. Zandt, Implications of crustal property variations for models of Tibetan Plateau evolution. *Nature* **387**, 37–43 (1997).
82. Q. Wang, C. J. Hawkesworth, D. Wyman, S.-L. Chung, F.-Y. Wu, X.-H. Li, Z.-X. Li, G.-N. Gou, X.-Z. Zhang, G.-J. Tang, W. Dan, L. Ma, Y.-H. Dong, Pliocene-quaternary crustal melting in central and northern Tibet and insights into crustal flow. *Nat. Commun.* **7**, 11888 (2016).
83. K. D. Nelson, W. Zhao, L. D. Brown, J. Kuo, J. Che, X. Liu, S. L. Klemperer, Y. Makovsky, R. Meissner, J. Mechie, R. Kind, F. Wenzel, J. Ni, J. Nabelek, C. Leshou, H. Tan, W. Wei, A. G. Jones, J. Booker, M. Unsworth, W. S. F. Kidd, M. Hauck, D. Alsdorf, A. Ross, M. Cogan, C. Wu, E. Sandvol, M. Edwards, Partially molten middle crust beneath southern Tibet: Synthesis of project INDEPTH results. *Science* **274**, 1684–1688 (1996).
84. M. J. Unsworth, A. G. Jones, W. Wei, G. Marquis, S. G. Gokarn, J. E. Spratt; The INDEPTH-MT team, Crustal rheology of the Himalaya and southern Tibet inferred from magnetotelluric data. *Nature* **438**, 78–81 (2005).
85. Y. Yang, M. H. Ritzwoller, Y. Zheng, W. Shen, A. L. Levshin, Z. Xie, A synoptic view of the distribution and connectivity of the midcrustal low velocity zone beneath Tibet. *J. Geophys. Res.* **117**, B04303 (2012).
86. B. R. Hacker, M. H. Ritzwoller, J. Xie, Partially melted, mica-bearing crust in Central Tibet. *Tectonics* **33**, 1408–1424 (2014).

Downloaded from http://advances.sciencemag.org/ on December 10, 2020

Acknowledgments: We thank T. Deng for providing the unmanned aerial vehicle photo and R. Zhu for help with the initial paleomagnetic measurements. We also thank L. Ding, F. Chen, R. Gao, J. Sun, Q. Wang, J. Zhao, and D. He for comments on the manuscript and support. We thank the editors and anonymous reviewers and A. Yin for encouragement and comments that have greatly improved the manuscript. We thank H. Chang, S. Yang, K. Fu, S. Dai, Y. Miao, Y. Lu, Y. Chi, S. Tuo, Y. Chen, X. Wu, J. Zan, Z. Han, C. Chen, Z. Zhang, Y. Fang, and F. Wu for assistance in the field and laboratory. This paper is dedicated to the memory of Academician Prof. Li Jijun for his initial design and support and Prof. Gao Junping and Mr. Fang Xiaohui for their field and laboratory assistances. **Funding:** This work was co-supported by the National Second Expedition to the Tibetan Plateau (2019QZKK0707), the Strategic Priority Research Program of Chinese Academy of Sciences (XDA20070201), and the NSFC Basic Science Center for Tibetan Plateau Earth System (CTPES No. 41988101-01). G.D.-N. acknowledges funding from the ERC MAGIC grant 649081. **Author contributions:** X.F., G.D.-N., and C.W designed the research and wrote the manuscript with help from J.N. X.F., C.S., W.Z., and Y.C. conducted field investigations, sampling, and paleomagnetic measurements. Q.M. carried out zircon U-Pb dating. T.Z. and Z.M. joined the field sampling and analyzed the tuff and tuffite geochemistry, mineralogy, and petrography. **Competing interests:** The authors declare that they have no competing interests. **Data and materials availability:** All data needed to evaluate the conclusions in the paper are presented in the paper and/or the Supplementary Materials. Additional data related to this paper may be requested from the authors.

Submitted 30 December 2019
Accepted 19 October 2020
Published 9 December 2020
10.1126/sciadv.aba7298

Citation: X. Fang, G. Dupont-Nivet, C. Wang, C. Song, Q. Meng, W. Zhang, J. Nie, T. Zhang, Z. Mao, Y. Chen, Revised chronology of central Tibet uplift (Lunpola Basin). *Sci. Adv.* **6**, eaba7298 (2020).

Downloaded from http://advances.sciencemag.org/ on December 10, 2020

Science Advances

Revised chronology of central Tibet uplift (Lunpola Basin)

Xiaomin Fang, Guillaume Dupont-Nivet, Chengshan Wang, Chunhui Song, Qingquan Meng, Weilin Zhang, Junsheng Nie, Tao Zhang, Ziqiang Mao and Yu Chen

Sci Adv **6** (50), eaba7298.
DOI: 10.1126/sciadv.aba7298

ARTICLE TOOLS http://advances.sciencemag.org/content/6/50/eaba7298

SUPPLEMENTARY MATERIALS http://advances.sciencemag.org/content/suppl/2020/12/07/6.50.eaba7298.DC1

REFERENCES This article cites 81 articles, 17 of which you can access for free
http://advances.sciencemag.org/content/6/50/eaba7298#BIBL

PERMISSIONS http://www.sciencemag.org/help/reprints-and-permissions

Use of this article is subject to the Terms of Service

Science Advances (ISSN 2375-2548) is published by the American Association for the Advancement of Science, 1200 New York Avenue NW, Washington, DC 20005. The title *Science Advances* is a registered trademark of AAAS.

Copyright © 2020 The Authors, some rights reserved; exclusive licensee American Association for the Advancement of Science. No claim to original U.S. Government Works. Distributed under a Creative Commons Attribution NonCommercial License 4.0 (CC BY-NC).

Downloaded from http://advances.sciencemag.org/ on December 10, 2020